Tech Science Press

Chitosan/Nanocrystalline Cellulose Biocomposites Based on Date Palm (*Phoenix Dactylifera L.*) Sheath Fibers

Abeer M. Adel[1], Amira M. El-Shafei[2], Atef A. Ibrahim[1] and Mona T. Al-Shemy[1,*]

[1]Cellulose and Paper Department, National Research Center, 33El-Bohouth St. (Former El-Tahrir St.), Dokki, P.O. 12622, Giza, Egypt.

[2]Textile Research Division, National Research Center, 33El-Bohouth St. (Former El-Tahrir St.), Dokki, P.O. 12622, Giza, Egypt.

[*]Corresponding Author: Mona T. Al-Shemy. Email: mt.el-shemy@nrc.sci.eg.

Abstract: In this study, nanocrystalline celluloses were used to enhance physical, mechanical and water vapor barrier properties of chitosan films for potential food packaging applications. Two different mineral acids (sulfuric and phosphoric) were used to extract nanocrystalline cellulose from date palm sheath fibers. The influence of cellulose I and cellulose II on the properties of the isolated nanocrystalline celluloses (e.g., yield, energy and length of intra- and intermolecular hydrogen bonds, and degree of substitution) were studied too. The characteristics of chitosan biocomposite film with phosphorylated nanocrystalline cellulose were compared to those with sulfated nanocrystalline cellulose. Results showed that besides cellulose polymorphism, the ionic ester groups on the surface of nanocrystalline cellulose is one of the factors influencing the physical, chemical, mechanical, and water vapor barrier properties in chitosan/nanocrystalline cellulose biocomposites.

Keywords: Biocomposite; Cellulose I; Cellulose II; Nanocrystalline cellulose (NCC); physico-mechanical properties; Thermal stability

Abbreviations:

CI: Cellulose I

CII: Cellulose II

CS: Chitosan

DPS: Date palm sheath

NCC: Nanocrystalline cellulose

PNCC: Phosphorylated nanocrystalline cellulose

SNCC: Sulfated nanocrystalline cellulose

1 Introduction

Lignocellulosic materials, the most abundant natural resource on the earth, exhibit many advantages as compared to their synthetic counterparts including their being readily available, renewable, biodegradable, and toxicologically harmless with advantageous characteristics and significant importance for the industrial sector [1]. Cellulose, the major structural component of plant cell walls, is a linear polymer of D-anhydroglucose units linked together with β(1-4)-glycosidic bonds [2]. Cellulose I (CI), the most predominant crystalline form, consists of two simultaneous crystal phases, CI_α and CI_β. CI_α exists mainly in algae and bacteria while cellulose of higher plants is enriched in CI_β. Mercerization process has the ability to remove hemicellulose and impurities, resulting in inter-fibrillar regions in lignocellulosic fibers to become less dense and rigid. The entire fibers are converted into a swollen state accompanied by rupture

DOI: 10.32604/jrm.2019.00034

of microfibrils cellulose assembly and alignment. Consequently, the parallel chains of metastable CI irreversibly converted into antiparallel chains of stable cellulose II (CII) crystal structure [3,4].

Nanocrystalline celluloses (NCCs) are formed by breaking down the cellulose fibers and isolating the crystalline regions. The literature shows the importance of NCCs as their strength properties are much higher than those of several metallic and polymeric products available commercially. The production of NCCs via chemical treatments using strong acids (e.g., sulfuric [1] , nitric [5] , and hydrochloric acids [6]) have shown to be successful in hydrolyzing cellulose fibers. When the acid hydrolysis of cellulose takes place, highly crystalline rigid rod-like hydrophilic particles with nanoscale dimensions are produced. However, the use of sulfuric acid as a hydrolyzing agent is accompanied by several drawbacks. The sulfate groups introduced to the NCCs surface through sulfuric acid hydrolysis assist the degradation of cellulose at a temperature lower than its parent counterpart. This caused the insufficient thermal stability, leading to a negative effect on the possible applications of NCCs in thermo-nanocomposites [7]. Thus the use of mineral acids other than sulfuric acid for the hydrolysis of cellulose became a challenge. One of these mineral acids is phosphoric acid, which was revealed its possibility to be a promising substitute for sulfuric acid hydrolysis [8,9].

Recently, the possibility of obtaining biocomposite films with various functionalities were investigated by Chen and Liu [10] and Mandal and Chakrabarty [11]. It was shown that, the NCC potential role in biocomposite applications is focused on their mechanical properties as a nano-reinforcing phase and in the advanced functional applications is based on their exceptional properties. Incorporation of NCC into a wide range of polymeric matrices was attempted, including synthetic and natural ones (such as PLA or starch) [12,13]. Among various available biopolymer materials, chitosan (CS) has been given a considerable attention because of its unique properties such as; multiplicity, biodegradability and renewability [14]. However, biocomposites with CS have several draw backs such as sensitivity to water, high affinity to water permeability and moderate mechanical properties. Many literatures investigate the incorporation of another biopolymer to the CS biocomposite matrix to enhance its barrier and mechanical properties [15-17]. Many advantageous and various characteristics were obtained through binary CS/NCC biocomposite films [16,18,19]. On the biocomposite market, the combination of the physico-chemical properties from CS and NCC with known antibacterial property of CS on one hand and oxygen barrier property of NCC films alternatively, would make the utilize of these films in food and nonfood (surface coverings, packaging, medical) application fields relevant [14].

The main target of this study is to increase the economic value of the agricultural residues through converting them into needed high-value industrial products; which, in turn, decreases the environmental hazardous due to unsafe disposal of agricultural residues through combustion, and makes it possible to utilize the two acids (sulfuric or phosphoric) hydrolyzed NCCs from date palm sheath (DPS) raw material in biocomposite applications. To the best of our knowledge, there are no previous publications concerning the isolation of NCCs from DPS by sulfuric acid or phosphoric acid hydrolysis. Other works dealt only with the influence of polymorphism on the properties of sulfated NCCs and their biocomposite without extending the possible combined influence of other functional groups could be [20]. For this reason, in addition to the impact of polymorphism, the influence of ionic ester groups on the properties of the prepared NCC and CS/NCC biocomposite films has been studied as well. The prepared NCC samples were characterized using TEM, FTIR, XRD, TGA, zeta potential and particle size distribution measurements.

2 Experimental Section

2.1 Materials

Date palm (*Phoenix Dactylifera L.*) sheath fibers obtained from a local plantation in Egypt. CS with 90-95% degree of deacetylation and MW 400,000 was purchased from Oxford Laboratory, India. Sulfuric (97%) and phosphoric acids (85%) were supplied by AbcoChemie (ENG. Ltd) and Honeywell Specialty Chemicals (Seelze GmbH), respectively. Other reagents were of analytical grade and used without further purification.

2.2 Preparation of Sulfated and *Phosphorylated Nanocrystalline Cellulose (SNCC & PNCC)*

Before NCCs extraction, DPS fibers were subjected to successive purification steps of pulping, bleaching and mercerizing treatments to extract CI and CII fibers [21]. For SNCCs preparation, 1 g of CI and CII fibers were added to a preheated 6.5 M sulfuric acid solution (fiber to liquor ratio of 1:20) for 1.45 h at 50°C under strong agitation [22]. PNCCs were prepared by soaking 1 g of CI and CII fibers in distilled water for 15 min, and then vigorously blended with an electrically powered hand blender, until a pulp like slurry was obtained. Phosphoric acid (85% v/v) was slowly added (keeping the temperature below 25°C) until a phosphoric acid concentration of 10.7 M was reached. Then, the reaction vessel was placed in a preheated oil bath at 90°C, and the mixture stirred for 30 min [8]. The produced SNCC and PNCC fractions were continuously washed by the addition of distilled water and centrifuged until the solution conductivity reached ≈ 5 μ S cm^{-1} (pH 4). The SNCC and PNCC colloidal suspension were dialyzed against distilled water for 3-5 days, till reaching pH ≈ 7. The final SNCC and PNCC suspensions were subsequently undergone ultrasonic treatment for 30 min (Falc Instruments, LSB2, 59 kHz) in an ice bath.

All NCC suspensions prepared were filtered through sintered glass funnel No 1º before being lyophilized. The yields of the prepared NCCs were calculated as a percentage of the weight of the final products divided by the initial weights of the starting material (i.e., CI or CII DPS fibers). Tab. 1 shows yield % of NCCs obtained by sulfuric acid and phosphoric acid hydrolyses.

2.3 Preparation of CS Biocomposite Films

The biocomposite films were prepared by the solution casting method. CS solution was prepared by mechanically stirring 2% CS (wt/v) in 1% acetic acid solution (v/v) at 50ºC for 3 h. Biocomposite films were prepared by mixing CS solution with 7% (wt/wt CS) of lyophilized NCCI and NCCII. Glycerol (30% wt/wt CS) was added as plasticizer to the mixture after being homogenized at 13500 rpm for 5 min. The homogeneous mixture was magnetically stirred for 1 h at room temperature before being vacuum degassed. The films were casted into PTFE plates and subsequently dried in a vented oven at 38ºC for 24 h. Films were conditioned at 25ºC and 51% RH, using a chamber containing saturated $Mg(NO_3)_2$ solution, for 48 h before being tested.

2.4 Characterization and Instrumentation

Conductometric titration was performed to determine the degree of substitution. The lyophilized NCC samples (0.5 mg) were suspended in 0.01 M hydrochloric acid solution and the suspensions were titrated with 0.01 M NaOH. The change in conductivity was detected by 4510 conductivity meter (Jenway, UK). The degree of substitution was calculated by the following equation:

$$\mathbf{DS = (162 \times V_{eq} \times C_{NaOH})/(m - y \times V_{eq} \times C_{NaOH})}$$

where 162 g/mol^{-1} is the molar mass of an AGU, V_{eq} is the amount of NaOH in mL at the equivalent point, C_{NaOH} is the concentration (mol/L), and m is the oven-dried sample (g). *y* corresponds to the difference between the molecular weight of a charged and unsubstituted anhydroglucose unit. For SNCC, y = 80 g/mol, and for PNCC, y = 64 g/mol [23].

Zeta-potential and average size analyses of the prepared NCCs were carried out on a Malvern Nano Zeta-sizer (Malvern, Nano ZS, UK) at 20 ± 0.1°C. The average values were calculated from at least twelve runs.

FT-IR spectra of the prepared cellulosic samples and NCCs were recorded on JASCO FT-IR 6100 spectrometer (Tokyo, Japan). The absorbance measurements were carried out within the range of 4000-400 cm^{-1}, with 60 scans and a resolution of 4 cm^{-1}. All the measurements were carried out at least in duplicate. These samples were then lyophilized and analyzed as KBr pellets (1% cellulose in anhydrous KBr).

The energy of the hydrogen bonds (EH, kJ) was calculated with the following equation:

$$EH = 1/K [(\nu_0 - \nu)/\nu_0]$$

where ν_0 is the standard frequency corresponding to the free OH groups (3650 cm^{-1}), ν is the frequency of the bonded -OH groups (cm^{-1}), K = 1.6 × 10^{-2} $kcal^{-1}$. The length of hydrogen bonds (R) was determined on the basis of the frequency shift (Δν) of the OH absorption band, the quantity Δν is defined as (ν_0 - ν), according to the following equation [24]:

$$\Delta\nu = 4.43 \times 10^3 (2.84 - R)$$

The cellulosic samples were analyzed by Panalytical Empyrean X-ray diffractometer (PANalytical, Netherlands). The angle of incident monochromatic X-ray was within the range of 2θ = 5-40°. The crystallinity index was determined by Segal empirical equation.

$$Cr.I\ (\%) = [(I - I_{am}) / I] \times 100$$

where ***I*** is the overall intensity of the (200, 020) lattice peak at 2θ about 22.6° and 21.8°, respectively. I_{am} is the intensity of the amorphous material at 2θ about 18° where the intensity is minimum [25]. The crystallite sizes (*L)* were estimated using the well-known Scherrer equation.

$$L = K\lambda/\beta \cos\theta$$

where K is a constant with a value of 0.94, λ is the X-ray wavelength (0.1542 nm for Cu Ka radiation), β is the half height width of the diffraction peak, and θ is the Bragg angle corresponding to the (200) lattice plane in case of CI and (020) lattice plane in case of CII.

The thermo-gravimetric analyses (TGA) of the prepared samples were studied using a differential scanning calorimeter (SDT Q600 V20.9 Build 20). Measurements were carried out in an inert nitrogen atmosphere at a testing rate 10 °C min^{-1} and within a temperature range between 25 and 800°C.

Transmission electron micrographs of NCCs were taken with a high-resolution JEOL JEM-2100 Transmission Electron Microscope (Japan). The NCCs were deposited from an aqueous dilute dispersion on a micro grid covered with a thin carbon film (≈ 200 nm). The deposited fibers were subsequently stained with a 2% uranyl acetate solution to enhance the microscopic resolution.

The mechanical strength tests for CS biocomposite films were carried out using LLOYD LR 10k universal testing machine, England. The tensile specimens were cut in rectangular shapes with dimensions of 60 mm in length and 15 mm in width. The gauge length was fixed at 20 mm and the speed of the moving clamp was 10 mm/min. All tests were performed on a minimum of five samples and the reported results are average values.

Water vapor permeability (WVP) was determined according to ASTM E96-E80. Film specimens with approximately 5 cm diameter were mounted on the glass cups containing 1 g of anhydrous calcium chloride. Melted paraffin wax was used to fix the film specimen with the wide rim of the glass cup. They were weighed and then placed in desiccators containing saturated sodium chloride solution. The relative humidity of the chamber was kept at 75% and 25°C throughout the experiment. Weight gain of the cups covered with films was recorded daily for successive 5 days. The test was performed in triplicate. WVP was calculated by using the following equation:

$$WVP = W\ x/t\ A\ \Delta P$$

where (W/t) = the slope of the plot between weight loss and time, x = the average thickness of the films, A = the permeation area, and ΔP= the partial water vapor pressure difference of the atmosphere in the cup and saturated sodium chloride solution corresponding to 0-75% RH (i.e., 2.385 kPa).

3 Results and Discussion

3.1 The Chemical Composition of Raw DPS, CI and CII

The detailed chemical compositions of raw DPS and starting substrates used in this study (CI and CII DPS fibers) to prepare NCC were discussed clearly in our earlier published work [26].

The chemical composition of DPS fibers exhibits 73% holocellulose and 43% cellulose which is approximately equal to that of date palm rachis and *Posidonia oceanica* balls and higher than that of the date palm leaflet [27-29]. The lignin content (20.7%) is lower than those of date palm leaflet [27,28] and rachis [29]. The ash and extractives of DPS fibers (1.4% and 5.3%, respectively), when compared to the previously published studies, are lower than those of *Posidonia oceanica* balls and *Stipa tenacissima* alpha stem [29,30]. The cellulose content of CI and CII reached 81.5 and 95.6, respectively after bleaching and mercerizing treatment.

3.2 Characterization of Isolated NCCs

The recently established explanation describes the acid hydrolysis process as a heterogeneous reaction that involves the diffusion of acid into the cellulose fibers, followed by the breakage of glycosidic bonds [31]. During the hydrolysis process, a side reaction between the acid and surface hydroxyl groups of cellulose fibers takes place. The produced charged surface sulfate or phosphate esters help in improving dispersion of the NCC in water [32,33].

Tab. 1 presents yield %, zeta potential (ζ) and average particle size of NCCs obtained by sulfuric acid, and phosphoric acid hydrolysis. The reaction yield varied from 55.57 to 65.25 for CI and between 79.88 and 83.27 in case of CII. This can be easily explained by the higher cellulose content in CII substrate when compared to that of CI. It is worth noting that, the average yield obtained in this study is much higher than those obtained from *Posidonia oceanica* [34,35] and is comparable to that obtained from filter paper and Jute bast fiber [36,37].

The stability of NCC dispersions in aqueous media, which is an essential factor, was measured by zeta potential analysis. All the prepared NCC suspensions showed a negative ζ-potential in neutral water. The samples prepared by phosphoric acid hydrolysis with DS of 0.23, and 0.31 showed the lowest ζ-potential (-12.77 and -16.9 mV) for CI and CII polymorphs, respectively. The ζ-potential negative value rises when sulfuric acid is used. The highest recorded ζ-potential values were (-35.6 and -36.7 mV) for SNCCI and SNCCII with DS (0.25 and 0.36), respectively. The main reason for the high dispersion stability of NCCs prepared by sulfuric acid hydrolysis attributed to the presence of negatively charged sulfate groups on the surface of SNCC [33]. In case of phosphoric acid hydrolysis, the produced NCCs aggregate after shorter period of time. This may be related to the shortage of electrostatic repulsive forces between the crystalline particles of PNCCs [8].

In terms of particle sizes distribution, the specimens of NCCII were smaller than NCCI. The mercerization treatment preceding the hydrolysis process appeared to be valuable in decreasing the particle sizes. Such a state of interaction could be due to the easer chemical penetration through amorphous regions than crystalline regions [38]. Additionally, the increased internal surface area of CII with more stable antiparallel chains arrangement than the parallel one in the CI groups. Hence, smaller sizes of the particles were manifested by the higher availability of cellulose structures in CII polymorph [13,39]. The data given in Tab. 1 disclosed the larger particle size and width of PNCCs than SNCCs.

Table 1: Yield %, Zeta potential (ζ) and average particle size of NCCs obtained by sulfuric acid, and phosphoric acid hydrolysis

Sample	Yield %	ζ(mV)	Particle size	
			Size (d.nm)	Width (d.nm)
SNCCI	65.25±1.92	-35.6	30.36	8.81
SNCCII	83.27±0.70	-36.7	25.72	7.78

PNCCI	55.57±0.61	-12.7	94.77	16.42
PNCCII	79.88±0.41	-16.9	74.27	14.51

To investigate the effect of the two acids hydrolysis treatments on the morphology of NCCs and to confirm the separation of individual crystallites, diluted suspensions obtained after hydrolysis treatments were examined by TEM (Fig. 1). A comparison of the TEM microphotographs of NCCI and NCCII obviously confirmed the observed results of the particle size distribution. The particles of NCCII were considerably smaller and less aggregated than those of NCCI [20]. Also, NCCI has a rod or whisker shapes similar to CI, whereas NCCII comprises mixed rod and sphere shapes especially in the case of PNCCII. Thus, mercerization effectively affected the morphology and reduced the size of the cellulose crystals.

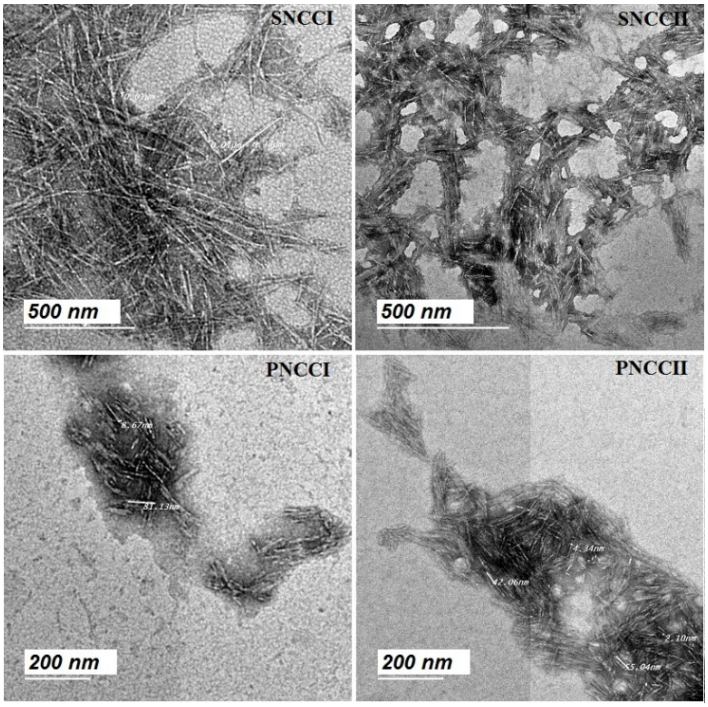

Figure 1: TEM graphs of: sulfated and phosphorylated NCCI and NCCII

The main infrared spectral differences between CI, CII and prepared NCCs, that allowed us to identify the structural changes in these samples, are shown in Fig. 2(a). The absorption bands around 3400, 2900, 1430, 1370, 890 cm^{-1} which are characteristics of native CI shifted to 3440, 2890, 1424, 1387, 884 cm^{-1} which are characteristic of CII [40]. The FT-IR spectra show that the acid hydrolysis reactions performed to obtain NCCI and NCCII from DPS fibers did not affect the chemical structure of the cellulosic fragments. This indicates that the chemical groups of the resulting materials were stable, and no strong chemical reaction occurred.

The highest absorption band of hydrogen-bonded OH stretching shifted to a lower wavenumber after the acid hydrolysis process (i.e., from 3418 cm^{-1} for CI to 3417, and 3414 cm^{-1} for SNCCI, and PNCCI, respectively, also from 3446 cm^{-1} for CII to 3444, and 3445 cm^{-1} for SNCCII, and PNCCII, respectively). These changes can associate with the disarrangement of intra- and intermolecular hydrogen bonds. The absorption band at 2900 cm^{-1} is related to CH_2 groups of cellulose [41]. According to other studies, the appearance of a band around 1645 cm^{-1} in all samples is related to the bending modes of water molecules due to a strong interaction between cellulose and water [42]. The enhancement of the absorption band in 1428-1433 cm^{-1} region, assigned to the symmetric CH_2 bending vibration, reflects an increase in the crystallinity degree of the samples [24]. The peak appeared in the range 1340-1383 cm^{-1} in the spectra of

all samples is attributed to the symmetric bending vibration of the C-H from CH deformation vibration, and CH_2 vibration [42]. The peak associated with C-H rocking vibration of cellulose (anomeric vibration, specific for β-glucosides) is observed in CI, CII, SNCC, and PNCC samples at 894-896 cm^{-1} [43]. The intensity of this band for CI, CII and NCCII were higher than those for NCCIs.

The main differences in FT-IR spectra between NCCI and NCCII samples are the shift of (1700-1600 cm^{-1}) bands. The band at about 1730 cm^{-1} in SNCCI could be due to the presence of C-O linkage arising from carboxyl absorption due to the opened terminal glucose rings, oxidation of the C-OH groups and/or may be due to the C-O-O vibrations of the unconjugated carboxyl group of pectins, which were not removed during cellulose preparation [20]. The collected data of the length of intra- and intermolecular hydrogen bonds (R), and the energy of hydrogen bonds (EH) corresponding to the untreated and treated CI and CII polymorphs listed in Tab. 2. We can observe that the hydrogen bonds length of NCCIs become slightly smaller with higher energy than its parent counterpart CI polymorph, while NCCIIs hydrogen bonds length become a slightly longer with lower hydrogen bond energy than its corresponding parent CII polymorph. Implying that, all the bands influenced by the changes of intra- and inter-molecular bonds related to the transformation [24,44].

Table 2: The length and energy of hydrogen bonding, XRD, TGA and DTG data of cellulose polymorphs and CNCs obtained by sulfuric acid, and phosphoric acid hydrolysis

Sample	R (nm)	EH (kcal)	$L_{002,\,020}$ (nm)	*CrI*	T_{onset} (°C)	T_{max} (°C)	CR_{500} (wt%)
CI	2.7876	3.9726	7.3449	80	319	354	00.00
SNCCI	2.7874	3.9897	10.2310	82	227	272	21.74
PNCCI	2.7867	4.041	9.8457	83	315	347	6.411
CII	2.7933	3.5445	5.0237	81	320	356	14.51
SNCCII	2.7935	3.5274	5.2508	86	250	282	22.52
PNCCII	2.7937	3.5103	5.6026	85	319	351	19.8

The XRD was studied to determine the effect of the different acids treatments using sulfuric acid and phosphoric acid on the crystalline shape of the isolated NCCs. From Figs. 2(b) & 2(c), we can see that, the CI fibers exhibited lattice peaks at 2θ = 14.86 ($1\bar{1}0$), 16.08 (110), 22.58 (200) and 34.18 (004) which assigned to CI, while after mercerization treatment (CII), the main crystalline peak (200) split into two obvious peaks at 2θ = 20.13 (110) and 2θ = 21.66 (020) indicating the formation of CII structure [45]. Preserving the polymorphism of each NCCI and NCCII asserts that the acidic hydrolysis treatment does not affect the polymorphic form of NCCs. However, after degradation and defibrillation of the fibers to a nano-scale range, the crystallinity index and the average crystallites size of NCCs turned into larger as can be seen in Tab. 2. The diffraction patterns of NCCI exhibited one intense peak at 2θ = 22.56 (200), a broad overlapped peak at 2θ = 15.51 ($1\bar{1}0$), 15.82 (110) and a weak peak at 2θ = 34.8 (004). Moreover, NCCII exhibited two intense peaks at 2θ = 19.92 (110) and 2θ = 21.71 for (020) peak, and two weak peaks at 2θ = 12.01 ($1\bar{1}0$) and 2θ = 34.43 for (004) plan. The comparable crystallinity indices and crystallite size for each crystal form of the sulfated and phosphorylated NCCs confirm that the crystalline core of the whiskers is not affected by the acid hydrolysis treatment, which is therefore limited only to the crystal surfaces as previously found [46].

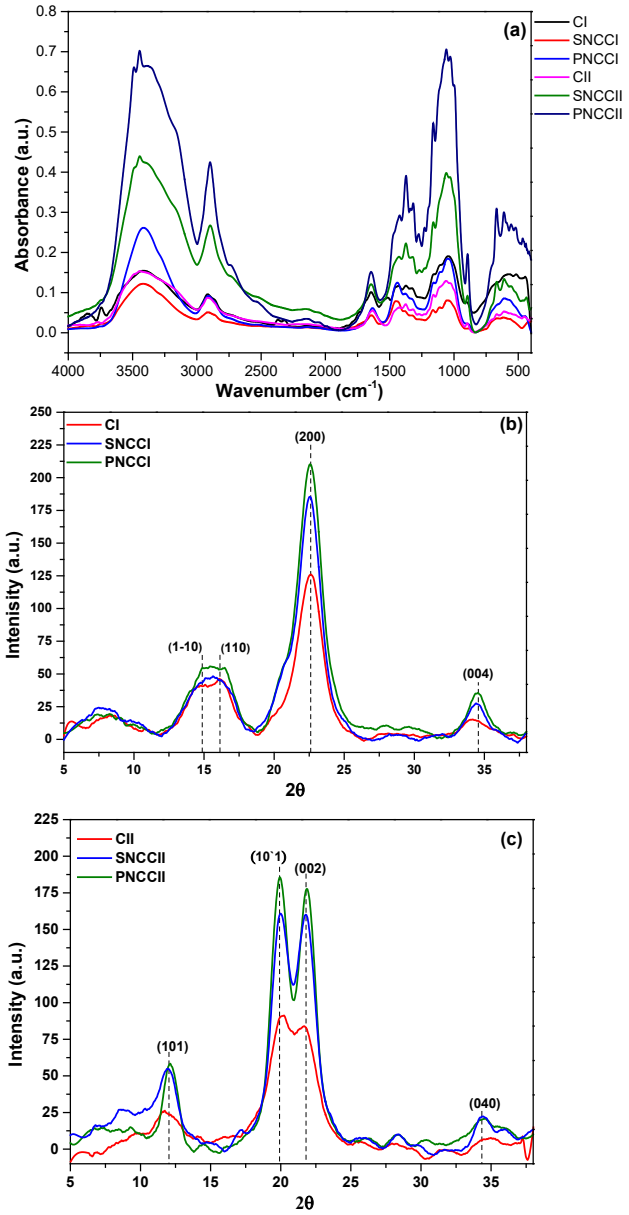

Figure 2: FT-IR spectroscopy (a) and XRD patterns (b, C) of: CI, CII, sulfated and phosphorylated NCCI and NCCII

The thermo-gravimetric (TG) and derivative thermo-gravimetric (DTG) curves of CI, CII and NCCs fibers are shown in Fig. 3. The thermal behavior of cellulosic materials depends mainly on their chemical composition, structure, and degree of crystallinity [47]. All samples had a small weight loss at a temperature lower than 120°C, corresponding to the evaporation of the moisture in the samples. At higher temperature range, the pyrolysis process of all samples takes place. Tab. 2 lists the onset temperature (T_{onset}, °C), degradation temperature (T_{max}, °C), and char residue (*CR,* %) at 500°C. The results of the thermal stability clearly indicated that, T_{max} decreased by the acid hydrolysis treatment. This could be ascribed to the increase in the surface area exposed to the thermal degradation. The degradation of CI, CII, SNCCII and PNCCI, II displayed one pyrolysis process. Whereas, the degradation of SNCCI follow a different mechanism which is displayed by the presence of a hump in near of the DTG curves. The first process prevails the whole pyrolysis. The two-step pyrolysis of SNCCI could be due to the presence of sulfate groups on the crystal

surface [48,49]. Consequently, upon their thermal degradation, a char acting as flame retardant protecting the interior of the crystal is formed. Furthermore, the occurrence of the second step of thermal degradation from about 315 to 550°C may be related to the breakdown of the interior of un-sulfated crystals [43,49]. However, NCCs showed typical cellulose degradation with an T_{onset} of 227 and 315 °C for SNCCI, and PNCCI, correspondingly, while NCCIIs had T_{onset} of 250 and 319°C, for SNCCII, and PNCCII, respectively. *CRs* of CI and CII samples were 0.00 and 14.51%, respectively. The level of the β-glycosidic linkages in the CII stable structure is reflected by the dramatic increase in its *CRs* [50]. *CRs* were 19.8 and 22.52 wt% for PNCCII and SNCCII respectively; however, it was only 6.411 wt% and 21.74 wt% for PNCCI, and SNCCI each. The difference between NCCs and their parental counterpart in *CRs* could attribute to nano-crystals with much smaller particle size and higher numbers of free end chains. At lower temperatures, the end chains start to decompose, which facilitate the CRs increase. SNCCII and PNCCII have the highest CRs because of the dual effect of the flame retardant sulfate and phosphate ester groups and CII polymorph structure, serving apparently as a protective barrier to both mass and energy from the burning surface to the attached polymeric chains [43,48]. The higher *CRs* produced by SNCC as compared to PNCC are probably due to the higher surface fictionalization and the lower temperature required for degradation of SNCC. This manifests a greater heterogeneity of the sample due to the different content of sulfate groups integrated on the cellulose surface. More sulfated fractions of cellulose degraded at lower temperatures, while fractions less penetrated by the sulfate groups tend to become more thermally stable [8].

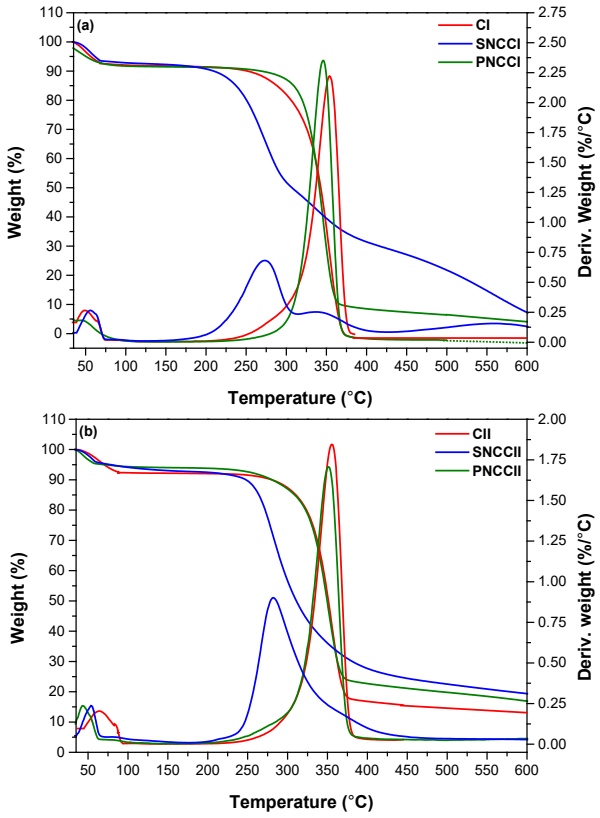

Figure 3: TGA and DTG of (a) CI and (b) CII polymorphs of SNCC and PNCC

3.3 Characterization of CS Biocomposite Films

Based on our previous study [21], CS biocomposite films were made from 7% NCC blends. From Tab. 3, we can notice that films made from NCCI had higher tensile strength than those made from NCCII. The irregular shapes of cellulose nano-particle provide mechanical interlocking to strengthen CS films. Also, the presence of sulfate and phosphate groups on NCC surface may increase the polar-polar interaction between the NCC themselves and CS particles and consequently increases the mechanical properties of films made from those NCC samples. The difference in mechanical properties of NCCI and NCCII biocomposites is probably due to the difference in their particle morphology, aspect ratio and/or hydrogen bonding capability.

The effect of NCCI and NCCII with different functionality on WVP of CS biocomposite films is manifested in Tab. 3. The presence of NCCs with different functionality and aspect ratios is thought to enhance the tortuosity in the CS films by a different rate, leading to slower water vapor diffusion processes and therefore, to a lower permeability [51]. WVP of CS biocomposite film decreased significantly by loading with SNCCI. However, the variance of WVP with SNCCII loading might be due to the higher fractions of the available hydroxyl groups from antiparallel arrangement of CII polymorph which in turn may lead to the aggregation of NCCs particles at 7% loading and consequently forming voids in the composite matrix. The variation of water vapor barrier property between PNCCI and PNCCII is much smaller than those between SNCCI and SNCCII. One possible reason could attribute to the high affinity of phosphate ester groups on the NCCs surface to water vapors.

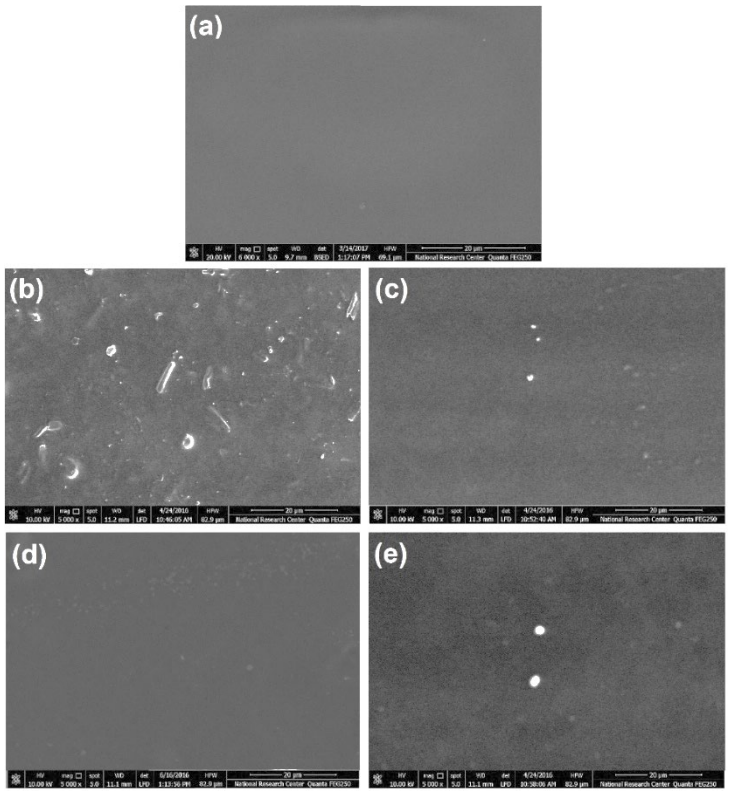

Figure 4: Surface morphology of (a) pristine CS, (b) CS/SNCCI, (c) CS/SNCCII, (d) CS/PNCCI and CS/PNCCII biocomposite films

Fig. 4 illustrates the surface microstructures of the CS/NCC biocomposite films loaded with sulfated and phosphorylated NCCs. All CS/NCC biocomposite films were with uniform thickness and smooth, without any macroscopic bubbles, cracks, or pores. Unlike the smooth and homogenous surface of pristine

CS film (Fig. 4(a)), the addition of NCC leads to rough surface with a decreased smoothness and homogeneity. In biocomposites with NCCII polymorph, NCCs approximately were well distributed in the polymeric matrix with small flakes or dots that tend to accumulate on the film surface (Figs. 4(b), 4(c), 4(d) & 4(e)). However, NCCI polymorph dispersion was not uniform and many agglomerations covered the surface of the film especially in the case of SNCCI. At the acidic pH of the film solution, NCCs in the suspension are prone to aggregate through the polymer matrix because of the removal of surface sulfate groups, the high interfacial area, and the surface energy.

Fig. 5 shows the differences in chemical functionality between the FT-IR spectra of CS/SNCC, and CS/PNCC biocomposite films. All films showed characteristic bands of pristine CS film. For CS/SNCC biocomposite, the presence of sulfated groups was confirmed by new bands at (1261, 1269 cm^{-1}) and (859, 824 cm^{-1}) associated with the asymmetrical S = O vibration and the asymmetrical C-S-O (C-SO_3^-) vibration, respectively [52]. The CS/PNCCI film has two new bands; at 2356cm^{-1} and 1336 cm^{-1} assigned to the P-H stretching vibration mode, and the P = O stretching mode of the incorporated phosphate groups, respectively. In case of CS/PNCCPII film, three new bands related to the P-H stretching vibration, the P=O stretching and P-OH stretching vibration modes were detected at 2255, 1338 and 932 cm^{-1}, respectively [52,53]. Beside phosphate groups, also carboxylate groups were confirmed with new detectable band at 1768 cm^{-1}. This could be attributed to the partial oxidation of the cellulose units during the phosphorylation process.

The absorption intensity of crystalline-sensitive band at 1440 cm^{-1} (CH_2) was increased by embedding of NCCs, while amorphous peak at 898 cm^{-1} almost disappeared, indicating its crystalline components were much higher compared to the pristine CS film.

The X-ray diffraction patterns of the pristine CS film and CS/NCC biocomposite films with different NCCs are indicated in Fig. 5. The diffractogram of pristine CS and biocomposite films showed 2 broad halo peaks at 2θ = 5-12.5º and 15-25º. These broad halo peaks indicate a semi-crystalline structure signifies a combination of crystalline and amorphous peaks [54].

From the XRD pattern of CS biocomposite films with PNCCI, the incorporation of NCC into CS films changes peak position of pristine CS slightly to higher 2θº with a decrease in the peak intensity and the d-spacing among the sheets. Since the structure of pristine CS is semi-crystalline and the proportion of NCC is very low (7%), the diffraction pattern of NCC can be overcome by that of CS. Similar results have been reported for CS based biocomposite films with nanofibrillated cellulose [19], bacterial cellulose [18], and oxidized nanocellulose [16]. Contrast to what we previously expected, the XRD pattern of CS biocomposite films with SNCCI, SNCCII, and PNCCII, reveals the changes of peak position of pristine CS to higher 2θº (near to the range of NCC peaks) with an increased intensity and decreased d-spacing among the sheets. The significant changes in the peaks position may be due to the higher crystallinity of the embedded NCCs. In other words, the dispersed phase of NCC in those films showed its own crystalline peaks in the CS matrix.

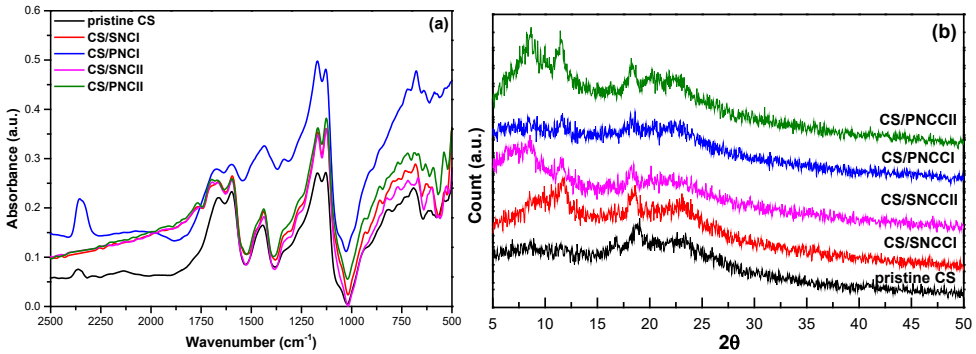

Figure 5: FT-IR spectroscopy (a) and XRD patterns (b) of pristine CS and CS biocomposite films loaded with sulfated and phosphorylated NCCI and NCCII

To evaluate the effect of different NCCs (SNCC and PNCC) and cellulose polymorphism (CI and CII) on the thermal stability of CS biocomposite films, the TGA and DTG were investigated. Fig. 6 demonstrates the TGA and DTG curves of CS biocomposite films with the different functionalized NCCs. Tab. 3 gives the summary for thermal parameters including T_{onset} Cº, T_{max} Cº, *Wloss %, and* CR_{700}%.

Generally, the presence of hydrogen bonding interactions between CS and NCC in each blend can be confirmed through thermal analysis according to the following observation:

- The thermogram of each CS/NCC film show only one main T_{onset} (if no interaction exists between the two polymers, which have different T_{onset} and T_{max}, the thermogram of the blends would show its thermal degradation in two different stages).
- The T_{onset} and T_{max} of the blends lie between the pristine CS and the pure NCC powder. These results deduced that these two polymers are well mixed together (T_{onset} and T_{max} of the blends change slightly with the different NCCs addition).

Based on the obtained results a correlation between tensile and thermal properties of CS/NCC biocomposite films can be found as the thermal stability of the CS/NCC biocomposite was observed to be enhanced by the increase of TS and decrease of EB.

The first weight loss ($Wloss_1$) appeared below 150ºC is due to the evaporation of absorbed water moisture and residual acetic acid [55]. The major weight loss ($Wloss_2$) occurred at temperature range between 200-400ºC, was attributed to the rapid decomposition of the polymer segments of CS and NCC due to the thermal scission of the polymers backbone [55].

According to the DTG curves, the appearance of a right shoulder to the peak of the second degradation stage (T_{max2}) could be due to the complex network formed in biocomposite films via strong non-covalent interactions between the surface functionality of NCC (sulfate and phosphate ester groups on the surface of SNCC and PNCC, respectively) and the macromolecular chains of CS polymer after their incorporation into the polymer matrix. When comparing thermal properties of CS biocomposite films with NCCI and NCCII polymorphs it can be seen that, the biocomposites with NCCI polymorphism show a higher thermal stability than those with NCCII polymorphism. This result is opposite to what was previously expected, since NCCII showed a higher thermal stability than NCCI. However, this difference seems to be compensated by the higher mechanical properties of CS/NCCI biocomposite. Along with our finding in earlier study, it can be deduced that the chemical functionality, mechanical strength and NCC polymorphism, as those properties showed different results improvement of CS/NCC biocomposite films, are correlated to thermal stability [21].

Table 3: Mechanical, TGA and DTG parameters of pristine CS and CS biocomposite films loaded with sulfated and phosphorylated NCCI and NCCII

Films	TS (MPa)	EB %	YM (MPa)	$WVP \times 10^{-3}$ (g/m.day.kPa)	T_{onset1} (ºC)	T_{max1} (ºC)	T_{onset2} (ºC)	T_{max2} (ºC)	$Wloss_1$ (wt%)	$Wloss_2$ (wt%)	CR_{700} (wt%)
Pristine CS	16.74 ± 1.87	50.80 ± 5.31	113.65 ± 12.60	2.51	119	159	223	280	16.21	44.07	25.92
CS/SNCCI	35.45 ± 1.83	54.65 ± 6.90	281.01 ± 27.33	0.99	132	173	247	282	15.1	42.59	24.57
CS/SNCCII	24.40 ± 1.33	40.79 ± 7.19	395.19 ± 32.04	2.11	137	176	209	280	14.72	47.98	21.72
CS/PNCCI	35.40 ± 2.90	63.80 ± 6.90	369.52 ± 37.03	1.89	127	170	246	282	12.35	44.45	26.25
CS/PNCCII	32.41 ± 3.02	77.80 ± 7.40	209.75 ± 29.56	2.18	133	178	209	275	16.34	46.91	21.72

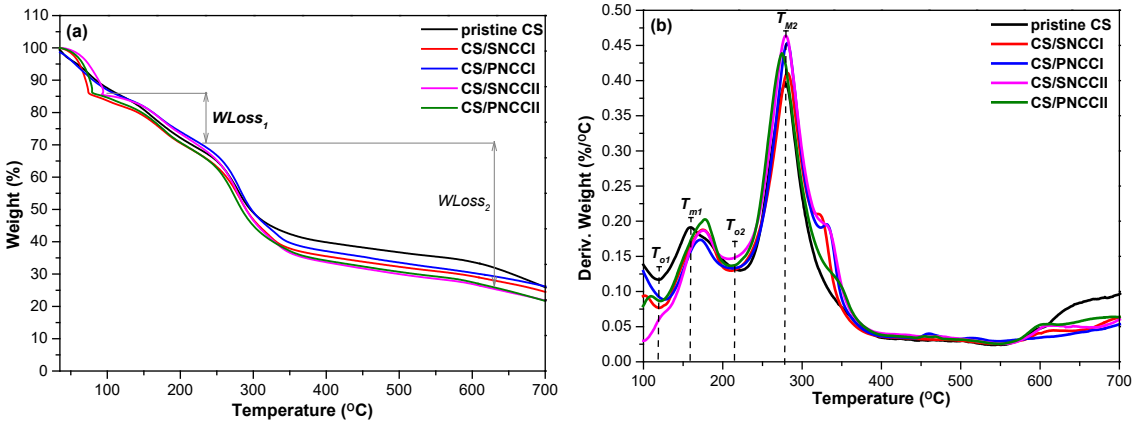

Figure 6: TGA (a) and DTG (b) of pristine CS and CS biocomposite films loaded with sulfated and phosphorylated NCCI and NCCII

4 Conclusion

In this study, the aqueous suspensions of NCCs from CI and CII have been successively prepared after sulfuric and phosphoric acid hydrolysis. Consequently, negatively charged sulfate or phosphate groups are formed via an esterification process between the acid and the surface hydroxyl groups of NCC. The TEM microphotographs of NCCIs and NCCIIs clearly confirmed that the particles of NCCII were particularly smaller and less aggregate than those of NCCI. NCCIs showed a fibrillar or whisker shapes, in contrast to NCCIIs which form mixed spherical or irregular particles. SNCCI and SNCCII are more stable in water suspensions than PNCCI, II. The thermal results revealed that NCCII samples have better thermal stability properties than NCCIs. Also, NCCs prepared using phosphoric acid were more thermally stable than NCCs prepared by sulfuric acid which is promising for the future application in thermo biocomposite. X-ray diffraction results of NCCs prepared by the two acids hydrolysis showed a comparable crystallinity index and crystallite size for each crystalline form. The mechanical and WVP analysis tests for CS biocomposite with NCCs show an enhancement in mechanical and barrier properties than the pristine CS film. The degree of the enhancement vary with the variation of the functional ester group (sulfate or phosphate) and polymorphism of NCCs. Hence, based on the obtained results we can prove that both functional groups and polymorphism influence the properties of NCCs which in turn affect the mechanical, water vapor permeability and thermal properties of CS/NCC biocomposites.

Acknowledgment: Financial support for this research is by the National Research Center, Giza, Egypt.

References

1. Martínez-Sanz, M., López-Rubio, A., Fabra, M. J., Lagaron, J. M. (2014). A new method for developing industrially viable nanocrystalline cellulose-based nanocomposites via melt compounding. *Journal of Renewable Materials, 2,* 107-117.
2. Zhang, Y., Nypelö, T., Salas, C., Arboleda, J., Hoeger, I. C. et al. (2013). Cellulose nanofibrils. *Journal of Renewable Materials, 1,* 195.
3. Langan, P., Nishiyama, Y., Chanzy, H. (1999). A revised structure and hydrogen-bonding system in cellulose II from a neutron fiber diffraction analysis. *Journal of the American Chemical Society, 121(43),* 9940-9946.
4. Dinand, E., Vignon, M., Chanzy, H., Heux, L. (2002). Mercerization of primary wall cellulose and its implication for the conversion of cellulose I→cellulose II. *Cellulose, 9(1),* 7-18.

5. Zhang, P. P., Tong, D. S., Lin, C. X., Yang, H. M., Zhong, Z. K. et al. (2014). Effects of acid treatments on bamboo cellulose nanocrystals. *Asia-Pacific Journal of Chemical Engineering, 9(5),* 686-695.
6. Yu, H., Qin, Z., Liang, B., Liu, N., Zhou, Z. et al. (2013). Facile extraction of thermally stable cellulose nanocrystals with a high yield of 93% through hydrochloric acid hydrolysis under hydrothermal conditions. *Journal of Materials Chemistry, A1(12),* 3938-3944.
7. Filson P. B., Dawson-Andoh, B. E. (2009). Sono-chemical preparation of cellulose nanocrystals from lignocellulose derived materials. *Bioresource Technology, 100(7),* 2259-2264.
8. Camarero Espinosa, S., Kuhnt, T., Foster, E. J., Weder, C. (2013). Isolation of thermally stable cellulose nanocrystals by phosphoric acid hydrolysis. *Biomacromolecules, 14(4)*, 1223-1230.
9. Li, S., Li, C., Li, C., Yan, M., Wu, Y. et al. (2013). Fabrication of nano-crystalline cellulose with phosphoric acid and its full application in a modified polyurethane foam. *Polymer Degradation and Stability, 98(9),* 1940-1944.
10. Chen, G., Liu, B. (2013). Cellulose sulfate based film with slow-release antimicrobial properties prepared by incorporation of mustard essential oil and β-cyclodextrin. *Food Hydrocolloids, 55*, 100-107.
11. Mandal, A., Chakrabarty, D. (2015). Characterization of nanocellulose reinforced semi-interpenetrating polymer network of poly(vinyl alcohol) & polyacrylamide composite films. *Carbohydrate Polymers, 134,* 240-250.
12. Abdul Khalil, H. P., Davoudpour, Y., Islam, M. N., Mustapha, A., Sudesh, K. et al. (2014). Production and modification of nanofibrillated cellulose using various mechanical processes: a review. *Carbohydrate Polymers, 99*, 649-665.
13. Mariano, M., El Kissi, N., Dufresne, A. (2014). Cellulose nanocrystals and related nanocomposites: review of some properties and challenges. *Journal of Polymer Science Part B: Polymer Physics, 52(12),* 791-806.
14. Dehnad, D., Mirzaei, H., Emam-Djomeh, Z., Jafari, S. M., Dadashi, S. (2014). Thermal and antimicrobial properties of chitosan-nanocellulose films for extending shelf life of ground meat. *Carbohydrate Polymers, 109,* 148-154.
15. HPS, A. K., Saurabh, C. K., Adnan, A. S., Fazita, M. N., Syakir, M. I. et al. (2016). A review on chitosan-cellulose blends and nanocellulose reinforced chitosan biocomposites: properties and their applications. *Carbohydrate Polymers, 150*, 216-226.
16. Soni, B., Hassan el, B., Schilling, M. W., Mahmoud, B. (2016). Transparent bionanocomposite films based on chitosan and TEMPO-oxidized cellulose nanofibers with enhanced mechanical and barrier properties. *Carbohydrate Polymers, 151,* 779-789.
17. Xu, Y. X., Kim, K. M., Hanna, M. A., Nag, D. (2005). Chitosan-starch composite film: preparation and characterization. *Industrial Crops and Products, 21(2),* 185-192.
18. Fernandes, S. C., Oliveira, L., Freire, C. S., Silvestre, A. J., Neto, C. P. et al. (2009). Novel transparent nanocomposite films based on chitosan and bacterial cellulose. *Green Chemistry, 11(12),* 2023-2029.
19. Fernandes, S. C., Freire, C. S., Silvestre, A. J., Neto, C. P., Gandini, A. et al. (2010). Transparent chitosan films reinforced with a high content of nanofibrillated cellulose. *Carbohydrate Polymers, 81(2),* 394-401.
20. Borysiak, S., Grząbka-Zasadzińska, A. (2016). Influence of the polymorphism of cellulose on the formation of nanocrystals and their application in chitosan/nanocellulose composites. *Journal of Applied Polymer Science, 133(3).*
21. Adel, A. M., El-shafie, A. M., Al-Shemy, M. T., Ibrahim, A. A., Rabia, A. E. G. M. (2017). Influence of cellulose polymorphism on tunable mechanical and barrier properties of chitosan/oxidized nanocellulose bio-composites. *Egyptian Journal of Chemistry, 60(4),* 639-652.
22. Pasquini, D., Teixeira, E. D. M., Curvelo, A. A. D. S., Belgacem, M. N., Dufresne, A. (2010). Extraction of cellulose whiskers from cassava bagasse and their applications as reinforcing agent in natural rubber. *Industrial Crops and Products, 32(3),* 486-490.
23. Huang, P., Zhao, Y., Kuga, S., Wu, M., Huang, Y. (2016). A versatile method for producing functionalized cellulose nanofibers and their application. *Nanoscale, 8(6),* 3753-3759.
24. Ciolacu, D., Ciolacu, F., Popa, V. I. (2011). Amorphous cellulose-structure and characterization. *Cellulose Chemistry and Technology, 45(1),* 13.
25. Segal, L., Creely, J., Martin, A., Conrad, C. (1959). An empirical method for estimating the degree of crystallinity of native cellulose using the X-ray diffractometer. *Textile Research Journal, 29(10),* 786-794.

26. Adel, A., El-Shafei, A., Ibrahim, A., Al-Shemy, M. (2018). Extraction of oxidized nanocellulose from date palm (Phoenix Dactylifera L.) sheath fibers: influence of CI and CII polymorphs on the properties of chitosan/bionanocomposite films. *Industrial Crops and Products, 124,* 155-165.
27. Bendahou, A., Habibi, Y., Kaddami, H., Dufresne, A. (2009). Physico-chemical characterization of palm from Phoenix Dactylifera-L, preparation of cellulose whiskers and natural rubber-based nanocomposites. *Journal of Biobased Materials and Bioenergy, 3(1),* 81-90.
28. Bendahou, A., Dufresne, A., Kaddami, H., Habibi, Y. (2007). Isolation and structural characterization of hemicelluloses from palm of Phoenix dactylifera L. *Carbohydrate Polymers, 68(3),* 601-608.
29. Khiari, R., Mhenni, M. F., Belgacem, M. N., Mauret, E. (2010). Chemical composition and pulping of date palm rachis and Posidonia oceanica-a comparison with other wood and non-wood fibre sources. *Bioresource Technology, 101(2),* 775-780.
30. Marrakchi, Z., Khiari, R., Oueslati, H., Mauret, E., Mhenni, F. (2011). Pulping and papermaking properties of Tunisian Alfa stems (Stipa tenacissima)-Effects of refining process. *Industrial Crops and Products, 34(3),* 1572-1582.
31. Bai, W., Holbery, J., Li, K. (2009). A technique for production of nanocrystalline cellulose with a narrow size distribution. *Cellulose 16(3),* 455-465.
32. Brito, B. S. L., Pereira, F. V., Putaux, J. L., Jean, B. (2012). Preparation, morphology and structure of cellulose nanocrystals from bamboo fibers. *Cellulose, 19(5),* 1527-1536.
33. Bondeson, D., Mathew, A., Oksman, K. (2006). Optimization of the isolation of nanocrystals from microcrystalline cellulose by acid hydrolysis. *Cellulose, 13(2),* 171.
34. Bettaieb, F., Khiari, R., Hassan, M. L., Belgacem, M. N., Bras, J. et al. (2015). Preparation and characterization of new cellulose nanocrystals from marine biomass Posidonia oceanica. *Industrial Crops and Products, 72,* 175-182.
35. Bettaieb, F., Khiari, R., Dufresne, A., Mhenni, M. F., Belgacem, M. N. (2015). Mechanical and thermal properties of Posidonia oceanica cellulose nanocrystal reinforced polymer. *Carbohydrate Polymers, 123,* 99-104.
36. Lu, Z., Fan, L., Zheng, H., Lu, Q., Liao, Y. et al. (2013). Preparation, characterization and optimization of nanocellulose whiskers by simultaneously ultrasonic wave and microwave assisted. *Bioresource Technology, 146,* 82-88.
37. Cao, X., Ding, B., Yu, J., Al-Deyab, S. S. (2012). Cellulose nanowhiskers extracted from TEMPO-oxidized jute fibers. *Carbohydrate Polymers, 90(2),* 1075-1080.
38. Mwaikambo, L. Y., Ansell, M. P. (2002). Chemical modification of hemp, sisal, jute, and kapok fibers by alkalization. *Journal of Applied Polymer Science, 84(12),* 2222-2234.
39. Habibi, Y. (2014). Key advances in the chemical modification of nanocelluloses. *Chemical Society Reviews, 43(5),* 1519-1542.
40. Yu, L., Lin, J., Tian, F., Li, X., Bian, F. (2014). Cellulose nanofibrils generated from jute fibers with tunable polymorphs and crystallinity. *Journal of Materials Chemistry, A2(18),* 6402-6411.
41. Cheng, M., Qin, Z., Liu, Y., Qin, Y., Li, T. et al. (2014). Efficient extraction of carboxylated spherical cellulose nanocrystals with narrow distribution through hydrolysis of lyocell fibers by using ammonium persulfate as an oxidant. *Journal of Materials Chemistry, A2(1),* 251-258.
42. Jonoobi, M., Khazaeian, A., Tahir, P. M., Azry, S. S., Oksman, K. (2011). Characteristics of cellulose nanofibers isolated from rubberwood and empty fruit bunches of oil palm using chemo-mechanical process. *Cellulose, 18(4),* 1085-1095.
43. Li, R., Fei, J., Cai, Y., Li, Y., Feng, J. et al. (2009). Cellulose whiskers extracted from mulberry: a novel biomass production. *Carbohydrate Polymers, 76(1),* 94-99.
44. Ciolacu, D., Chiriac, A. I., Pastor, F. I., Kokol, V. (2014). The influence of supramolecular structure of cellulose allomorphs on the interactions with cellulose-binding domain, CBD3b from Paenibacillus barcinonensis. *Bioresource Technology, 157,* 14-21.

45. Okano, T., Sarko, A. (1985). Mercerization of cellulose. II. Alkali-cellulose intermediates and a possible mercerization mechanism. *Journal of Applied Polymer Science, 30(1),* 325-332.
46. Habibi, Y., Chanzy, H., Vignon, M. R. (2006). TEMPO-mediated surface oxidation of cellulose whiskers. *Cellulose, 13(6),* 679-687.
47. Rosli, N. A., Ahmad, I., Abdullah, I. (2013). Isolation and characterization of cellulose nanocrystals from Agave angustifolia fibre. *BioResources, 8(2),* 1893-1908.
48. Haafiz, M. K., Hassan, A., Zakaria, Z., Inuwa, I. M. (2014). Isolation and characterization of cellulose nanowhiskers from oil palm biomass microcrystalline cellulose. *Carbohydrate Polymers, 103,* 119-125.
49. Mandal, A., Chakrabarty, D. (2011). Isolation of nanocellulose from waste sugarcane bagasse (SCB) and its characterization. *Carbohydrate Polymers, 86(3),* 1291-1299.
50. Abbott, A., Bismarck, A. (2010). Self-reinforced cellulose nanocomposites. *Cellulose, 17(4),* 779-791.
51. Sanchez-Garcia, M., Gimenez, E., Lagaron, J. (2008). Morphology and barrier properties of nanobiocomposites of poly (3-hydroxybutyrate) and layered silicates. *Journal of Applied Polymer Science, 108(5),* 2787-2801.
52. Liu, P., Borrell, P. F., Bozic, M., Kokol, V., Oksman, K. et al. (2015). Nanocelluloses and their phosphorylated derivatives for selective adsorption of Ag(+), Cu(2+) and Fe(3+) from industrial effluents. *Journal of Hazardous Materials, 294,* 177-185.
53. Wanrosli, W. D., Rohaizu, R., Ghazali, A. (2011). Synthesis and characterization of cellulose phosphate from oil palm empty fruit bunches microcrystalline cellulose. *Carbohydrate Polymers, 84(1),* 262-267.
54. Khan, A., Khan, R. A., Salmieri, S., Le Tien, C., Riedl, B. et al. (2012). Mechanical and barrier properties of nanocrystalline cellulose reinforced chitosan based nanocomposite films. *Carbohydrate Polymers, 90(4),* 1601-1608.
55. Shankar, S., Rhim, J. W. (2016). Preparation of nanocellulose from micro-crystalline cellulose: the effect on the performance and properties of agar-based composite films. *Carbohydrate Polymers, 135,* 18-26.